Influence of substitutional atoms on the diffusion of oxygen in dilute iron alloys

X. Wang,[1,2,*] M. Posselt,[1] and J. Faßbender[1,2]
[1]*Helmholtz-Zentrum Dresden–Rossendorf, Institute of Ion Beam Physics and Materials Research, Bautzner Landstraße 400, 01328 Dresden, Germany*
[2]*Technische Universität Dresden, 01062 Dresden, Germany*

(Received 9 May 2018; revised manuscript received 26 July 2018; published 21 August 2018)

A multiscale approach including density functional theory (DFT) and atomistic kinetic Monte Carlo (AKMC) simulations is applied to investigate the diffusion of interstitial oxygen atoms in bcc Fe under the influence of substitutional foreign atoms (Al, Si, P, S, Ti, Cr, Mn, Ni, Y, Mo, and W). The substitutional atoms can be assumed to be immobile since their diffusion coefficient is much smaller than that of oxygen. First, jumps of oxygen in pure bcc Fe between first-, second-, and third-neighbor octahedral interstitial sites are investigated. It is found that the first-neighbor jump is most relevant, with the tetrahedral site as the saddle point. The second-neighbor jump consists of two consecutive first-neighbor jumps. The barrier for a direct third-neighbor jump is too high to be significant for the diffusion process. In the presence of substitutional atoms the most important migration paths are first-neighbor jumps between modified octahedral sites with modified tetrahedral sites as saddle points. Calculations show that Si, P, Ni, Mo, and W cause some modifications of the migration barriers of oxygen and their interaction with O is mainly repulsive. Al, Cr, and Mn have a significant influence on the barriers and they exhibit strong attractive interactions with O. The most important modification of the barriers is found for S, Ti, and Y where deep attractive states exist. Based on the migration energies obtained by DFT, AKMC simulations on a rigid lattice are employed to determine the diffusion coefficient of oxygen in a dilute iron alloy containing the different substitutional atoms. It is found that Si, P, Ni, Mo, and W have almost no influence on the diffusivity of O. The presence of Al, Cr, Mn, S, Ti, and Y causes a significant reduction of the mobility of oxygen. In these cases the temperature dependence of the oxygen diffusion coefficient shows considerable deviations from an Arrhenius law. These phenomena are discussed in detail by considering the occupation time for the different states. The present findings on the strong dependence on the kind of substitutional atoms change the picture of oxygen diffusion in dilute iron alloys substantially.

DOI: 10.1103/PhysRevB.98.064103

I. INTRODUCTION

Diffusion of foreign atoms such as dopants, impurities, and alloying elements, which occurs during fabrication, processing, and operation of functional materials, has a crucial influence on materials properties. Most of the previous experimental and theoretical studies on this phenomenon were focused on the migration of a single atomic species in a pure host material. Different atomic-scale mechanisms were found, such as diffusion via interstitial sites and by means of intrinsic point defects, i.e., vacancies and self-interstitial atoms. However, the migration of one foreign atom may be influenced by the presence of other foreign atoms of the same or another type, even if the concentration of foreign atoms of different kinds is still rather low.

Iron-based ferritic alloys are widely used in industrial applications. They always contain several foreign atoms or solutes. Some of them are impurities; others are purposely introduced in order to improve the mechanical properties, the corrosion and radiation resistance, as well as the high-temperature stability. Many research activities are focused on the understanding of nanostructure evolution in these materials, under thermal and/or mechanical load and under irradiation. Multiscale modeling can substantially contribute to improve the knowledge on these processes. The general scheme is the following: First, data on migration barriers and binding energies of foreign atoms in bcc Fe are determined. Most advantageous and correct is the determination of these quantities by first-principles density functional theory (DFT). In a second step kinetic Monte Carlo simulation or rate theory is applied using the data determined in the first step as inputs. Atomistic kinetic Monte Carlo (AKMC) simulation on a rigid lattice is a very suitable method in order to gain insight into many details of nanostructure evolution. Most of these simulations use rather simplified models in order to describe the migration barriers of foreign atoms (see, e.g., the review paper of Becquart and Domain [1]). Since these barriers are the most important ingredients to describe the kinetics of a system, the results of that kind of simulations may be not sufficiently correct. Even in a multicomponent ferritic alloy containing foreign atoms with a rather low concentration the influence of many different local atomic environments on the migration barrier should be taken into account precisely. This requires a huge effort since a very high number of barriers must be determined by DFT calculations. Recently, Messina *et al.* [2] presented an elegant neural-networks-based AKMC method

*Present address: Helmholtz-Zentrum Dresden–Rossendorf, Bautzner Landstraße 400, 01328 Dresden, Germany; x.wang@hzdr.de

to overcome these problems. Previous DFT and AKMC work on nanostructure evolution in bcc Fe was mainly related to the diffusion of substitutional solutes which migrate via the vacancy mechanism. Simonovic *et al.* [3] and Liu *et al.* [4] performed combined DFT and AKMC calculations on the effect of different substitutional solutes on the diffusion of carbon in bcc Fe via interstitial sites. Barouh *et al.* [5] and Shang *et al.* [6] considered the influence of vacancies on the migration barriers of the interstitial solutes carbon, nitrogen, and oxygen by means of DFT. Ortiz *et al.* [7] investigated the influence of carbon on He migration and clustering in bcc Fe using DFT and rate theory. Grigorev *et al.* [8] studied the mobility of H-He clusters in W using molecular dynamics with interatomic potentials. In particular they considered the influence of H on the mobility of He as part of the mixed clusters. Besides these first-principles-based and atomistic works, papers using a thermodynamics-based method with material parameters from literature to treat the influence of traps on interstitial diffusion are worth mentioning (see, e.g., Ref. [9] and references therein).

In the present paper DFT calculations and AKMC simulations are applied to investigate the diffusion of oxygen in bcc Fe under the influence of foreign atoms on substitutional sites, such as Al, Si, P, S, Ti, Cr, Mn, Ni, Y, Mo, and W. This paper is motivated by gaining fundamental diffusion data which are hardly obtainable by experiments, and by several practical applications. Oxygen plays a crucial role in the corrosion of iron-based alloys. It is also an important element in the formation and evolution of Y-Ti-O nanoclusters in nanostructured ferritic Fe-Cr alloys, which are considered as promising candidates for structural materials of future fusion and fission reactors [10]. It is known from literature that in bcc Fe the most stable position of O is the octahedral interstitial site and the tetrahedral interstitial site is the saddle point for first-neighbor jumps [4,6,11–13]. In the present paper it is investigated how the presence of foreign atoms modifies the O migration. First, jumps of oxygen in pure bcc Fe between first-, second-, and third-neighbor octahedral interstitial sites are investigated by DFT. Then, DFT is applied to determine the binding energy between oxygen and a foreign atom, for different neighbor distances, and to calculate the modified migration barriers, i.e., for the oxygen jump between the first and the second neighbor of a foreign atom, etc. Using the migration barriers obtained by DFT the diffusion coefficients of oxygen are determined by AKMC simulations considering a dilute iron alloy on a rigid lattice. Finally, the influence of the different foreign atoms on the oxygen diffusivity is discussed in detail.

II. DFT CALCULATIONS

A. Calculation method

The Vienna *ab initio* simulation package VASP [14–16] was applied to perform the DFT calculations. This code uses plane-wave basis sets and pseudopotentials generated within the projector-augmented wave approach [17,18] as well as the description of exchange and correlation effects by the Perdew-Burke-Ernzerhof parametrization [19] of the generalized gradient approximation. In all calculations the spin-polarized formalism was applied and a plane-wave cut-off of 500 eV was used. The Brillouin-zone sampling was performed employing the Monkhorst-Pack scheme [20]. The calculations were carried out for cubic bcc Fe supercells with 128 lattice sites and $3 \times 3 \times 3$ k points. For the integration in the reciprocal space the Methfessel-Paxton smearing method [21] was applied with a width of 0.2 eV. After introduction of an oxygen atom on an octahedral interstitial site and of another foreign atom on a substitutional site the positions of atoms as well as the volume and shape of the supercell were relaxed so that the total stress/pressure on the supercell became zero. Such calculations were performed for different distances between the oxygen and the foreign atom as illustrated in Fig. 1. The notation of the neighbor positions of oxygen relative to the foreign atom is according to the scheme for a simple cubic lattice (see Ref. [5]) which consists of the bcc lattice sites and the octahedral interstitial sites of the bcc lattice. Note that within this scheme oxygen cannot reside on third-neighbor, fourth-neighbor, seventh-neighbor, eighth-neighbor, etc., positions since these sites are already occupied by iron atoms, and note that there are two different ninth-neighbor sites (9a and 9b). The accuracy of DFT calculations is determined by two criteria: (i) If the residual force acting on any atom falls below a given threshold the relaxation calculation is stopped, and (ii) at each relaxation step the energy minimization is performed until the total-energy change falls below another threshold. In the present paper threshold values of 10^{-2} eV/Å and 10^{-5} eV are used, in the first and the second case, respectively. The binding energy between a foreign atom X on a substitutional site and the oxygen O on an octahedral interstitial site, at different distances to the foreign atom (see Fig. 1), is defined by

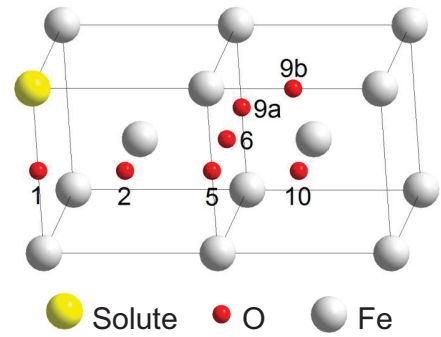

FIG. 1. Octahedral interstitial sites for oxygen in the neighborhood of a substitutional solute. The notation of oxygen positions relative to the foreign atom is according to the scheme for a simple cubic lattice that consists of the bcc lattice sites and the octahedral interstitial sites of the bcc lattice.

$$E_{\text{bind}} = E(X+O) + E_0 - E(X) - E(O). \quad (1)$$

$E(X+O)$, $E(X)$, and $E(O)$ denote the total energy of (iron) supercells with the defect pair $X+O$ and the monomers X and O, respectively, while E_0 is the total energy of the supercell with perfect bcc Fe. By definition the value of E_{bind} is negative in the case of attraction between the X and the O atoms.

The migration energy barriers and the minimum-energy paths for oxygen migration in bcc Fe were determined using the nudged elastic band (NEB) method [22,23], as implemented

in the vtsttools [24]. In this manner jumps of an oxygen atom between different octahedral interstitial sites in bcc Fe (with and without another foreign atom) were considered. In the NEB procedure the minimum-energy states before and after a jump are connected by a number of states or images that are constructed along the reaction path. Then, for these images a restricted relaxation is performed using the precision criteria mentioned above. After determining the minimum-energy path by the standard NEB procedure the climbing image NEB method is employed to ensure that the exact saddle point is found. The jump rate is given by

$$\nu = \nu_0 \exp\left(-\frac{E_m}{k_B T}\right), \tag{2}$$

with the migration energy barrier E_m and the attempt frequency ν_0. The latter quantity is determined by [25,26]

$$\nu_0 = \frac{k_B T}{h} \exp\left(-\frac{\Delta F^{\mathrm{vib}}_{\mathrm{mig}}(T)}{k_B T}\right), \tag{3}$$

where k_B and h are the Boltzmann and the Planck constant, respectively. The quantity in the exponential is the difference between the vibrational free energy of the supercell with the oxygen interstitial at the saddle point (SP) and that at the equilibrium position (octahedral interstitial site):

$$\Delta F^{\mathrm{vib}}_{\mathrm{mig}}(T) = F^{\mathrm{vib}}_{\mathrm{SP}}(T) - F^{\mathrm{vib}}_{\mathrm{min}}(T), \tag{4a}$$

$$F^{\mathrm{vib}}_{\mathrm{SP}}(T) = \sum_{i=1}^{3N-4} \left[\frac{1}{2} h\nu_{\mathrm{SP},i} + k_B T \ln\left(1 - \mathrm{e}^{-\frac{h\nu_{\mathrm{SP},i}}{k_B T}}\right)\right], \tag{4b}$$

$$F^{\mathrm{vib}}_{\mathrm{min}}(T) = \sum_{i=1}^{3N-3} \left[\frac{1}{2} h\nu_{\mathrm{min},i} + k_B T \ln\left(1 - \mathrm{e}^{-\frac{h\nu_{\mathrm{min},i}}{k_B T}}\right)\right]. \tag{4c}$$

$\nu_{\mathrm{SP},i}$ and $\nu_{\mathrm{min},i}$ are corresponding vibrational frequencies calculated by VASP and N is the number of atoms in the supercell.

In the high-temperature limit the Vineyard formula holds [27]:

$$\nu_0 = \frac{\Pi_{i=1}^{3N-3} \nu_{\mathrm{min},i}}{\Pi_{i=1}^{3N-4} \nu_{\mathrm{SP},i}}. \tag{5}$$

Note that before the vibrational frequencies are calculated the relaxation of the supercells must be performed with a very high precision. In the present paper the above-mentioned threshold values were 10^{-4} eV/Å and 10^{-7} eV.

B. Migration barriers of oxygen in pure iron and the attempt frequency

The octahedral interstitial site is the most stable site of oxygen in pure bcc Fe [11–13,28–30]. It was shown that the incorporation of O into the lattice leads to a local tetragonal distortion and a corresponding change of the supercell shape is observed if relaxation calculation is performed under zero stress/pressure conditions [30]. Three different migration paths of oxygen in pure bcc Fe were investigated in this paper: between (i) first-neighbor, (ii) second-neighbor, and (iii) third-neighbor octahedral sites. The results are shown in Fig. 2. The first-neighbor jump consists of a linear migration path with

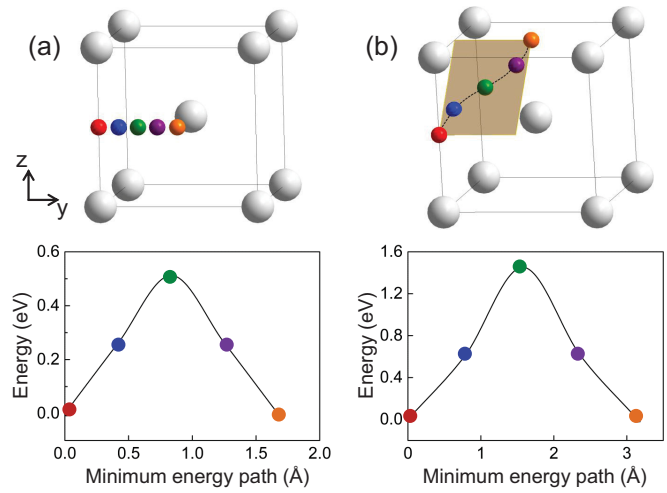

FIG. 2. Illustration of the minimum-energy paths for the jump of oxygen between first-neighbor (a) and third-neighbor (b) octahedral interstitial sites in pure bcc Fe.

a barrier of 0.512 eV. This value is consistent with previous DFT calculations of Fu *et al.* [11], Claisse and Olsson [13], Shang *et al.* [6], and Barouh *et al.* [5], who obtained 0.6, 0.48, 0.526, and 0.56 eV, respectively. The saddle point situated in the middle of the path corresponds to a tetrahedral interstitial site of the bcc lattice [see Fig. 2(a)]. Note that the data points correspond to the calculated values which are used to obtain the fit curve. It is worth mentioning that the tetragonal distortions in the initial and the final state differ: While in the initial state the elongation is along the z axis it is along the x axis in the final state. A tetragonal distortion is also observed at the saddle point. However, in this case the dimensions of the supercell in x and z directions are equal and slightly higher than in the y direction. It was found by NEB calculations that a second-neighbor jump consists of two successive first-neighbor jumps. This was also reported for carbon migration in bcc Fe [3] which occurs in a similar manner as the oxygen diffusion, i.e., between octahedral interstitial sites. The third-neighbor jump consists of a nonlinear migration path as shown in Fig. 2(b). The saddle point, a rhombohedral interstitial site, is in the middle of the minimum-energy path, with a barrier height of 1.452 eV. This result is also similar to the findings for carbon [3]. The barrier for the third-neighbor jump is considerably higher than that for a first-neighbor jump. For such a jump the probability of occurring is therefore much smaller than that for three consecutive first-neighbor jumps. Based on the above results, in the following only first-neighbor jumps are considered. For a first-neighbor jump the attempt frequency was determined according to the formalism outlined in Eqs. (4) and (5) and a value of 15.76 THz was obtained in the temperature range relevant for diffusion (above 500 K).

C. Binding energy of pairs consisting of an oxygen atom and a substitutional solute

The binding energies obtained after relaxation of a supercell with a foreign atom on a bcc site and oxygen on an octahedral interstitial site are summarized in Table I. Si, P, Ni, Mo, and W exhibit mainly repulsion and a few, very weak, attractive

TABLE I. Binding energy of oxygen-solute pairs at different distances (cf. Fig. 1). Negative (positive) values mean attraction (repulsion). DFT data from literature are given in brackets.

E_{bind} (eV)	1	2	5	6	9a	9b	10
O-Al	−0.243	0.047	−0.051	0.000	−0.04	−0.069	−0.030
O-Si	−0.064	0.453	0.051	−0.003	0.009	−0.081	0.017
O-P	0.051	0.161	0.071	−0.059	0.044	−0.024	0.040
O-S	−0.361	−0.466	−0.066	−0.134	0.051	0.062	0.013
O-Ti	−0.372 (−0.26 [12],−0.23 [13], −0.27 [28])	−0.593 (−0.55 [12], −0.45 [13], −0.55 [28])	−0.052 (0.07 [13])	−0.009 (0.14 [13])	−0.037 (0.12 [13])	0.094	−0.042
O-Cr	−0.257 (−0.25 [12], −0.1 [13])	−0.085 (0.02 [12],0.06 [13])	0.092 (0.2 [13])	0.025 (0.13 [13])	−0.003 (0.09 [13])	0.120	0.002
O-Mn	−0.246	−0.068	0.108	0.084	0.062	0.067	0.072
O-Ni	0.214	0.175	−0.02	0.015	−0.018	0.017	−0.028
O-Y	0.031 (0.35 [12],0.32 [13], 0.28 [28])	−1.010 (−1.01 [12],−0.73 [13], −0.85 [28])	−0.336 (0.04 [13])	−0.035 (0.07 [13])	−0.085 (0.11 [13])	0.217	−0.133
O-Mo	0.397	−0.048	0.057	0.056	−0.036	0.158	−0.037
O-W	0.555	0.075	0.075	0.065	−0.045	0.139	−0.042

interactions. In the case of Ni, Mo, and W highest repulsion exists at the first-neighbor distance, whereas for Si and P maximum repulsive interaction occurs at the second-neighbor distance. Al, Cr, and Mn show the strongest attraction at the first-neighbor distance while S, Ti, and Y show the highest attractive interaction with O at the second-neighbor distance. On the one hand Table I demonstrates that the interaction between O and the solutes has a relatively long range. On the other hand the trend is as expected, i.e., the interaction decreases with distances and approaches zero at the tenth-neighbor distance. An exception is the O-Y interaction that is still considerable at this distance. This may be explained by the large size of the Y atom which causes significant displacements and distortions. DFT data from literature are also given in Table I. These values show a very similar trend as the present results. However, the numbers are somewhat different, which should be mainly due to the fact that the literature data were obtained at constant volume of the supercell, whereas in the present paper not only the positions of atoms but also the size and shape of the supercell were relaxed until the total stress/pressure reached zero. Furthermore, in the present paper a newer version of VASP pseudopotentials (version 5.4) was used which may lead to some additional differences. Details on the volume change (compared to a supercell with perfect bcc Fe) and the distortion of the supercell by a single oxygen octahedral interstitial and by single substitutional solutes are given in the Supplemental Material [31]. The presence of oxygen leads to a considerable volume increase and to a tetragonal distortion. Most of the substitutional atoms cause an isotropic expansion of the supercell, whereas isotropic contraction is found for Si and P. Furthermore, the Supplemental Material [31] shows the effective volume change and the supercell distortion obtained for the different oxygen-solute pairs. The effective volume change, which is defined by the difference between the volume changes caused by the presence of the pair and the sum of the volume changes due to the presence of a single O atom and a single substitutional atom, can be positive or negative. Tetragonal and orthorhombic distortions of the supercell are observed which are caused by the presence of the oxygen interstitial and the spatial orientation of the O-solute pair. Tetragonal distortions are found for the first-, second-, sixth-, and ninth-neighbor distances since the relaxation occurs only in two spatial dimensions, because the initial geometrical arrangement of the pairs according to Fig. 1 is along [100], [110], [211], [221], and [300], respectively. On the other hand, in the case of pairs at fifth- and tenth-neighbor distances (oriented along [210] and [310]) orthorhombic distortions are observed due to relaxation in three dimensions.

The dependence of the binding energy of the oxygen-solute pair on the kind of the solute was investigated by studying the following characteristic quantities: (i) partial density of electronic states, (ii) magnetic moment, (iii) charge transfer, (iv) volume change of the supercell, and (v) distance between the two atoms belonging to the pair. It was found that the results concerning the charge transfer determined by Bader analysis [32] seem to be most suitable for a qualitative interpretation of the trends found for the binding energy. If the pair is at the first-neighbor distance in most cases attractive interaction occurs if the following two criteria are fulfilled simultaneously: Oxygen gains more than about 0.4 "electrons" and the solute loses more than about 0.6 "electrons." This indicates an ioniclike bond. With the exception of the O-S and the O-Y pair, in the other cases the ionic character of one of the partners is obviously not sufficiently pronounced for an attraction. More details about these investigations can be found in the Supplemental Material [31].

D. Oxygen migration barriers in the environment of a substitutional solute

Figure 3 shows the minimum-energy paths for the migration of oxygen between first-neighbor octahedral interstitial sites in the environment of different foreign atoms, up to the tenth neighbor. Due to the atomic configuration shown in Fig. 1

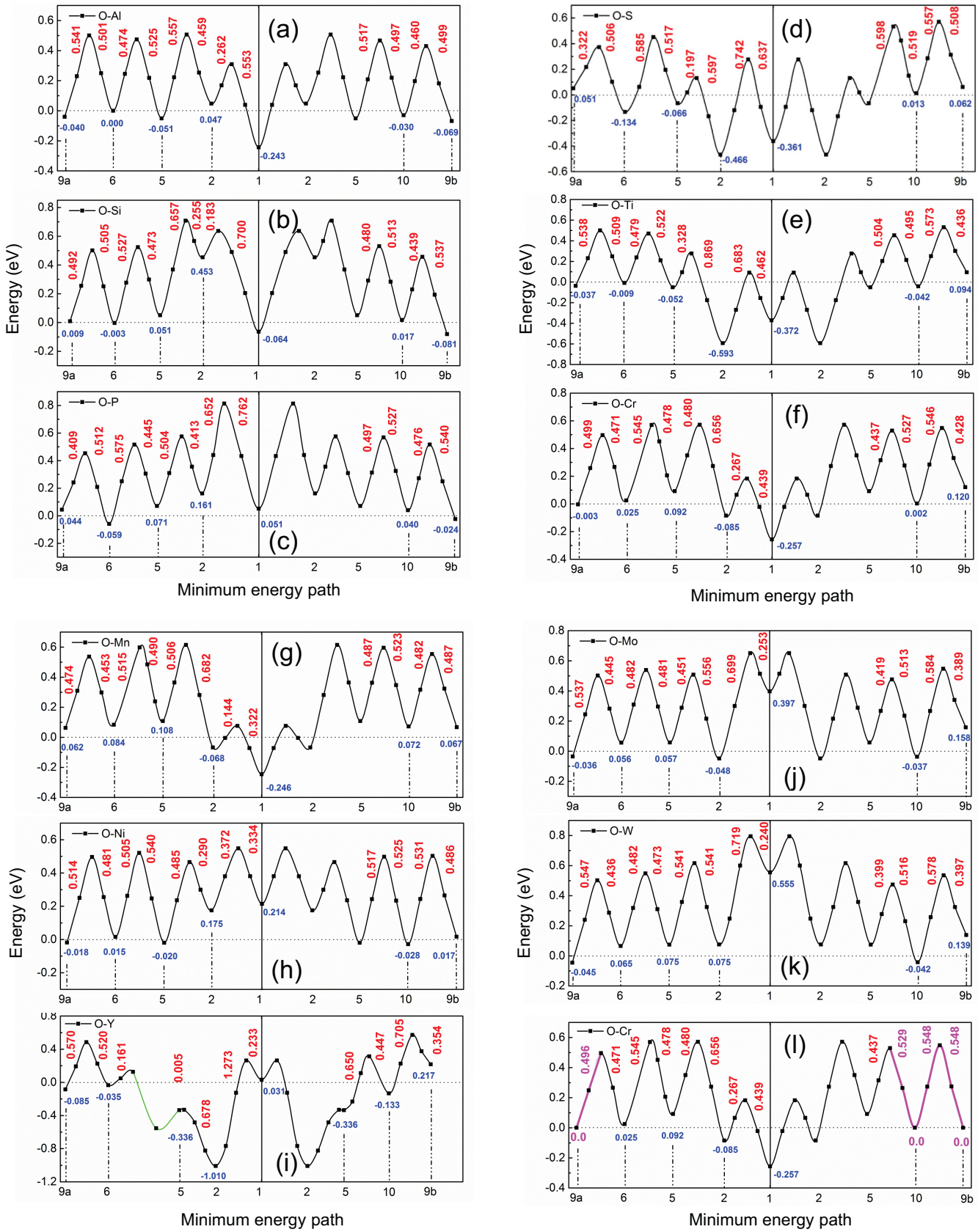

FIG. 3. Migration barriers for oxygen in the neighborhood of various substitutional atoms: Al (a), Si (b), P (c), S (d), Ti (e), Cr (f), Mn (g), Ni (h), Y (i), Mo (j), and W (k). The red and blue numbers show the barrier height and the binding energy, respectively. In AKMC simulations the barriers must be modified according to the detailed balance. This is illustrated in the case of Cr (l) where the changes are marked by magenta numbers and lines.

only the following first-neighbor jumps are possible: between neighbors 1 and 2, 2 and 5, 5 and 6, 5 and 10, 6 and 9, and 9b and 10. The migration barriers are higher or lower than the value of 0.512 eV obtained for pure bcc Fe. At the largest distance from the foreign atom the migration barriers approach this value. However, some differences remain, in particular in the case of Y which should be due to its atomic size. In the figures the data points depict the calculated values that are used to determine the fit curves. In the case of Ni most of the barriers are smaller and only a few are slightly higher than that in pure Fe. P, Mo, and W exhibit these kinds of barriers outside the second-neighbor shell whereas such barriers exist for Si outside the fifth-neighbor shell. However, in these cases the barriers for jumps into the closer environment of the foreign atom are relatively high (around 0.7 eV). Al, S, Ti, Cr, Mn, and Y show rather high barriers for escape from neighbor shells close to the solute, whereas the barriers for approaching are often relatively low. In the vicinity of S and Ti the escape is impeded by the combined action of the barriers for $2 \rightarrow 5$ and for $5 \rightarrow 6$ or $5 \rightarrow 10$ jumps. A similar situation exists for Al, Mn, and Cr caused by the combination of the barriers for the $1 \rightarrow 2$ and the $2 \rightarrow 5$ jump. Obviously, an impeded escape is correlated with the existence of deep attractive states. A special situation is found in the environment of Y. The NEB calculation for the transition between neighbor 5 and 6 shows a local minimum related to the first image and a local maximum related to the second image [see part of the line in Fig. 3(i) marked by green color]. Complete relaxation of the state corresponding to the local minimum led to the second-neighbor configuration. Thus one can conclude that a direct transition between neighbors 5 and 6 is not possible. On the other hand it can be assumed that the local maximum found between 5 and 6 is the barrier for a direct transition between neighbors 6 and 2. In the vicinity of Y the escape of the oxygen atom is strongly impeded by the combined action of the barriers for the $2 \rightarrow 5$ and $5 \rightarrow 10$ transitions. It should be noticed that calculations showed that O resides in a (meta)stable state at the fifth-neighbor position, with a shallow minimum which is hardly visible in Fig. 3(i). Note that there is also a very small barrier for the transition $5 \rightarrow 2$. With the exception of the peculiarities in the case of Y, in general the migration path of O is similar to that in pure bcc Fe, i.e., from a modified octahedral site via a modified tetrahedral site to another modified octahedral site. This is illustrated in Fig. 4 for the oxygen jump between the first- and second-neighbor position of Cr. In many plots shown in Fig. 3 the migration barrier corresponds to the middle data point in the graphical representation of the respective jump. Exceptions are the transitions between the first and second neighbors of Si, Y, and W, between the second and fifth neighbors of Y, between the fifth and tenth neighbors of S, between the fifth and sixth neighbors of Cr and Mn, and between neighbors 6 and 9a as well as 5 and 10 of Y. Also in these cases the saddle points correspond to modified tetrahedral interstitial configurations.

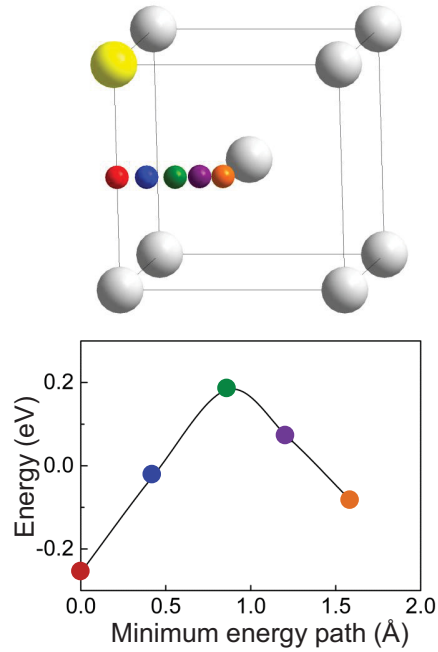

FIG. 4. Modified minimum-energy path for the jump of oxygen between the first and the second neighbor of Cr.

III. AKMC SIMULATIONS

A. Simulation procedure

A simple cubic (rigid) lattice consisting of bcc lattice sites as well as of the octahedral interstitial sites of the related bcc lattice is considered and three-dimensional periodic boundaries are used. The bcc sites are occupied by Fe atoms with the exception of one site that is occupied by a foreign atom. This site is chosen randomly and the foreign atom is assumed to be immobile since its diffusion coefficient (see Refs. [33,34]) is much smaller than that of oxygen. This assumption will be verified below. The concentration of foreign atoms in the alloy is determined by the size of the simulation cell. One oxygen atom is introduced on a randomly selected octahedral interstitial site. The AKMC step number and the physical time are set to zero at the beginning of the simulation. Based on the results presented in previous sections it is assumed that the migration of oxygen consists of jumps between first-neighbor octahedral sites. The main part of the AKMC code deals with the determination of possible foreign-atom neighbors of the oxygen atom before and after a jump. For this purpose linked cells and neighbor lists are used which are determined at the very beginning of the simulations. Based on the DFT data for E_m and ν_0 the jump rates for the four possible jumps of the O atom from a given octahedral site to neighboring octahedral sites are determined. Jumps from neighbor 9a, 9b, or 10 to larger distances, from larger distances to these sites, or jumps completely outside the ten neighbor shells are described as the jumps in pure Fe. In cases where at neighbor shells 9a, 9b, and 10 the binding energy between oxygen and the substitutional solute does not vanish, it is set to zero and the migration energy barriers $E_m^{9a,6}$, $E_m^{10,5}$, $E_m^{9b,10}$, and $E_m^{10,9b}$ are modified according to

$$E_m^{i,j} - E_m^{j,i} = E_{\text{bind}}^{j} - E_{\text{bind}}^{i}. \tag{6}$$

This relation describes the rule of detailed balance which must be fulfilled in AKMC simulations (see Ref. [35]). Note that Eq. (6) is always satisfied for transitions inside the tenth-neighbor shell. For illustration the modifications of $E_m^{9a,6}$,

$E_m^{10,5}$, $E_m^{9b,10}$, and $E_m^{10,9b}$ in the environment of Cr are shown in Fig. 3(l). Based on the jump rates ν_i ($i = 1...4$) determined for the four possible jumps to neighboring octahedral sites the cumulative function $\sum_{j=1}^{i} \nu_j$ as well as the probability $p_i = \sum_{j=1}^{i} \nu_j / \sum_{j=1}^{4} \nu_j$ are calculated. For all jumps the attempt frequency ν_0 is set equal to the value determined for a first-neighbor jump in pure bcc Fe (see Sec. II B). This introduces only a small error since the jump rates are mainly determined by the exponential function with the migration energy barriers which depend on the local atomic environment. A jump event k is selected using a random number r (uniformly distributed between zero and one): $p_{k-1} < r \leqslant p_k$. Then the jump is carried out, i.e., the position of the oxygen atom is changed. The AKMC step number is increased by 1 and the increase of the physical time is determined by $\Delta t = -\ln(r) / \sum_{j=1}^{4} \nu_j$, where r is another random number. Note that the migration of the O atom in the rigid lattice formed by bcc and octahedral sites is realized by changing the type of the occupation of octahedral sites (not occupied to occupied and vice versa). The procedure described above corresponds to the well-known rejection-free AKMC algorithm (see, e.g., Ref. [36]). It is carried out many times (MC steps) and the positions of the oxygen atom are recorded as a function of time. The number of Monte Carlo steps required for reliable results depends on the specific "landscape" of the migrations barriers (see Fig. 3). In any case several AKMC simulations were performed with increasing numbers of MC steps. If the diffusion coefficient does not further change, this value was considered to be the final result. In the present paper 10^6 to 10^{10} MC steps were used. In order to obtain good statistics the migration of the oxygen atom is simulated many times, with different initial positions of the oxygen and the foreign atom. The diffusion coefficients presented in this paper were calculated by averaging of the corresponding data that were determined in these independent simulations.

After the simulation of the migration of a given oxygen atom the diffusion coefficient is determined using the recorded data on position and time. In the present AKMC code the Guinan method [37–39] is used: The trajectory of the O atom is divided into n_s time segments δt, and for each segment m the squared displacement $sd(m) = [\vec{x}(t_m) - \vec{x}(t_{m-1})]^2$, with $t_m = t_{m-1} + \delta t$, is determined, where $\vec{x}$ denotes the position of the O atom at a given time. Applying the Einstein relation and averaging over all segments n_s leads to the O diffusion coefficient:

$$D = \frac{1}{n_s} \sum_{m=1}^{n_s} \frac{sd(m)}{6\,\delta t}. \tag{7}$$

Within certain limits, the size of the segments determined by δt or n_s can be chosen arbitrarily so that the calculation of the diffusion coefficient can be performed for many different subdivisions. It must be noticed that on the one hand δt must be sufficiently high ($\delta t \gg {\nu_0}^{-1}$) to include all local jump correlations, and on the other hand n_s should be also large enough to provide a statistically meaningful diffusion coefficient. In the present AKMC code the maximum and minimum values of n_s are 7500 and 10, respectively. The results show that too small (high) values of δt (n_s) lead to values of D which are not reliable, because correlations are not included sufficiently. In contrast, too high (small) values of δt (n_s) lead to large fluctuations of D which is due to poor statistics. Therefore, those values of D are not considered in the final averaging over the results for different subdivisions. In the present code the averaging is performed over subdivisions between $n_s^{\max}/3$ and $2n_s^{\max}/3$.

B. Diffusion coefficients of oxygen

AKMC simulations were performed to study oxygen diffusion in alloys with concentrations of substitutional solutes of 0.098, 0.231, 0.400, 0.781, and 1.852 at. %. As already mentioned above, in the present paper an AKMC simulation cell contains only one substitutional foreign atom, therefore the size of the cell ($8 \times 8 \times 8$, $6 \times 6 \times 6$, $5 \times 5 \times 5$, $4 \times 4 \times 4$, and $3 \times 3 \times 3$ bcc unit cells, respectively) is related to the solute concentration. With the exception of the case of highest concentration (1.852%) dilute alloys are considered. In dilute alloys the migration of the O atom cannot be influenced at the same time, or "simultaneously," by more than one substitutional solute or its periodic image. After leaving the region of influence of a certain solute atom, in a dilute alloy the diffusing O atom migrates (long enough) through perfect bcc Fe before it enters another region of influence. In present AKMC simulations the region of influence ends at the tenth-neighbor shell (see Fig. 3 and the discussion related to the detailed balance in the previous section). The concentration of 1.852% is already beyond that of a dilute alloy because there may occur a kind of "simultaneous interaction" of the O atom with the solute and its periodic image. This peculiar case will be discussed in detail later. Figure 5 shows the dependence of the diffusion coefficient on temperature in the range between 500 and 2000 K. It has to be taken into account that the presented data are strictly valid only in the ferromagnetic phase, i.e., below the Curie temperature (1043 K). Furthermore, at about 1183 K the α (bcc) to γ (fcc) transition of iron occurs. The main reason for showing a temperature scale up to 2000 K is to verify the expected convergence of the diffusion coefficient to the value for pure bcc Fe at sufficiently high temperatures. It must be also mentioned that in the present paper the temperature dependence of the spontaneous magnetization in the ferromagnetic state is neglected, i.e., it is always assumed that the magnetization of bulk iron corresponds to its ground-state value. According to the influence on the diffusion of oxygen the foreign atoms can be categorized into three groups, which is similar to the classification discussed concerning the migration barriers in Sec. II D. The first group consists of Si, P, Ni, Mo, and W. These solutes have a very small effect on the diffusion coefficient. The reason for this behavior is due to the size and combination of the migration barriers as depicted in Figs. 3(b), 3(c), 3(h), 3(j), and 3(k). The majority of barriers in the vicinity of Ni is somewhat lower than the barrier in pure Fe. Therefore, the diffusion coefficient increases slightly with concentration [see inset in Fig. 5(h)]. In the case of P, Mo, and W the barriers for oxygen jumps from the second to the first neighbor are rather high while the other barriers are not very different from that in pure iron. Similar conditions exist in the environment of Si with a high barrier between the fifth and the second neighbor. Such a combination of migration barriers, with a reduced accessibility of positions close to the solute,

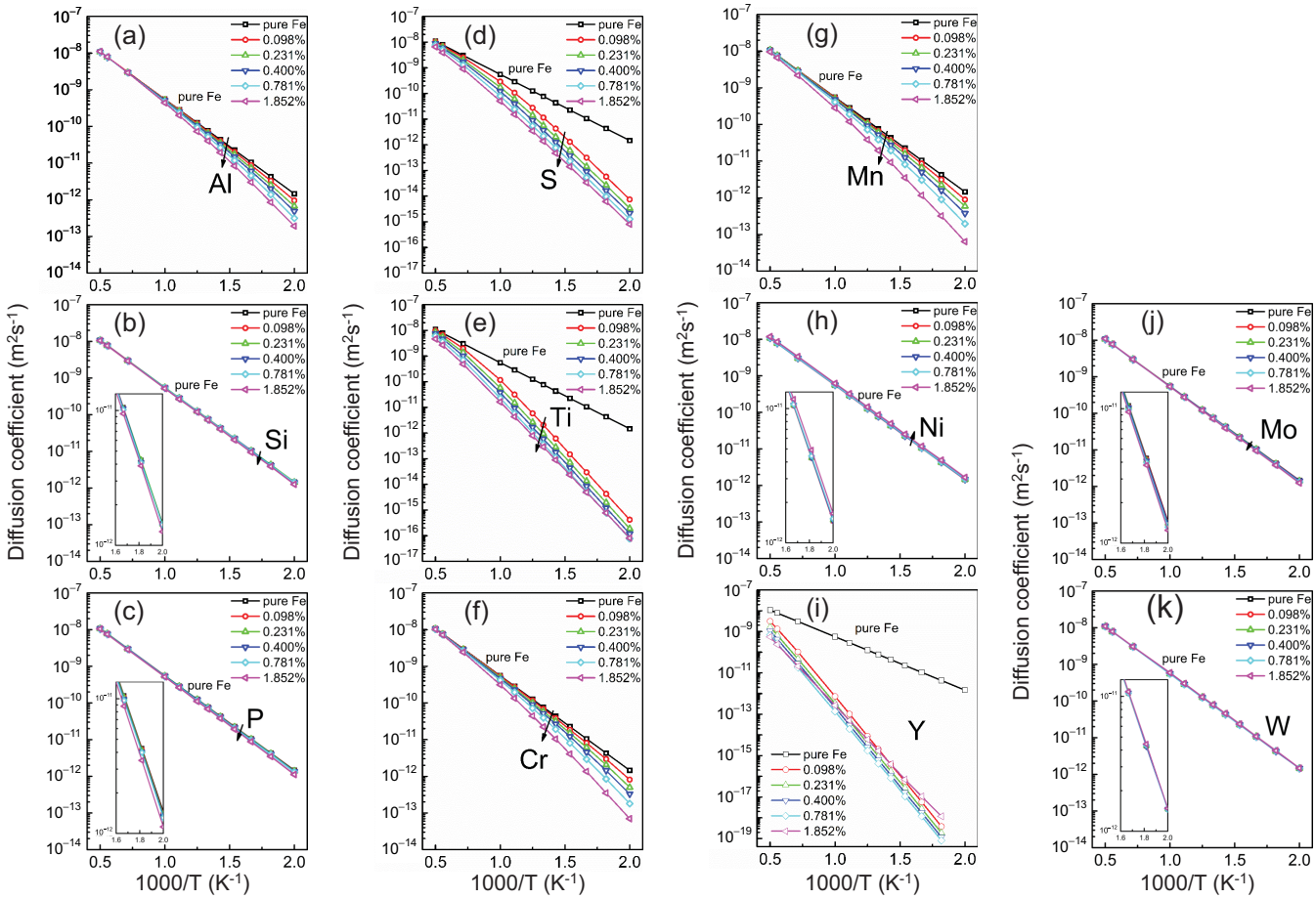

FIG. 5. Diffusion coefficient of oxygen in several dilute Fe alloys in dependence on temperature and solute concentration (in at. %).

may cause the so-called labyrinth mechanism [3,4], which leads to a slight reduction of the diffusion coefficient with increasing solute concentration [see insets in Figs. 5(b), 5(c), and 5(j)]. The second group of solutes with Al, Cr, and Mn exhibits a considerable reduction of oxygen mobility. Taking Cr as an example, 0.098% (1.852%) Cr decreases the diffusion coefficient by 44.3% (95.2%) at 500 K and by 2.6% (43.4%) at 1000 K, compared to the values for pure Fe. The reason for this behavior is the so-called trapping mechanism [3,4,9,40] caused by the existence of a pronounced attractive state at the first-neighbor distance and by high escape barriers from this state [see Figs. 3(a), 3(f), and 3(g)]. Such a trapping mechanism is also responsible for the huge decrease of the diffusion coefficient observed in the case of the third group with S, Ti, and Y. For example, the oxygen diffusivity decreases by 99.97% (99.99%) at 500 K and by 78.9% (97.05%) at 1000 K if the alloy contains 0.098% (1.852%) Ti. The foreign atoms S, Ti, and Y exhibit deep attractive states at the second-neighbor distance and the barriers for escape from these positions are very high [see Figs. 3(d), 3(e), and 3(i)]. However, in all cases considered in this paper the oxygen diffusion coefficient is still some orders of magnitude higher than that of the corresponding foreign atom (see Refs. [33,34,41]). Therefore, the assumption that the substitutional solute can be considered to be immobile in the AKMC simulations is justified.

It is not surprising that the influence of foreign atoms on the oxygen mobility leads to deviations from the Arrhenius behavior of the diffusion coefficient. This is clearly visible for solutes of the second and third group. The reason is the inhomogeneous distribution of the barrier heights: Specific barriers exist in the vicinity of the substitutional atom, while beyond the tenth-neighbor shell the migration barriers are equal to that in pure bcc Fe. The pronounced difference between all these barriers leads to a temperature dependence of the ratio between residence times in the various states. For a detailed study the ratio between the residence or occupation time of the oxygen atom at different neighbor distances and the total time of the simulation was determined. Figure 6 illustrates the residence time ratio for oxygen at the first-neighbor site of Cr and the second-neighbor site of Ti. Both sites are related to the highest absolute values of binding energy (see Table I). A strong variation with temperature and concentration is visible in Fig. 6. In the case of Cr the occupation time ratio continuously increases with concentration both at low and high temperature while it decreases with increasing temperature. The latter is due to the fact that with increasing temperature the ratio of the residence time in the deepest state to that in other states decreases because of the higher mobility of the diffusing atom. The reduction of the diffusion coefficient with concentration and the concave shape of the curves in Fig. 5(f) are related to the behavior of the occupation time ratio as shown in Fig. 6(a). The dependencies of the diffusion coefficient due to the presence of Al and Mn can be explained similarly to the case of Cr. The occupation time ratio for Ti [Fig. 6(b)] strongly

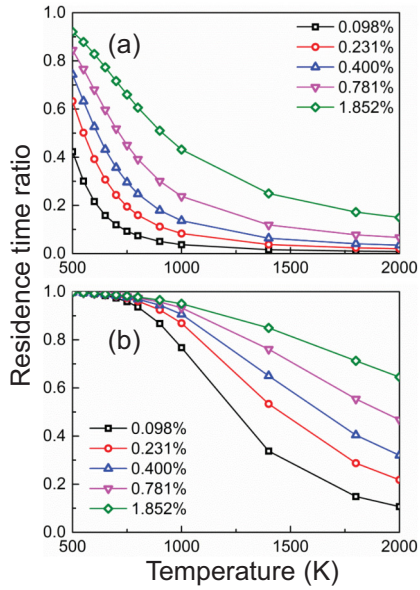

FIG. 6. Residence time ratio for oxygen at the first-neighbor site of Cr (a) and at the second-neighbor site of Ti (b).

differs from that of Cr. While this quantity also decreases with temperature, with increasing concentration a pronounced trend towards saturation is found at low temperature. This is the reason for the saturation of the reduction of the diffusion coefficient with increasing concentration observed at these temperatures [Fig. 5(e)]. At low temperature the residence time of oxygen at the second-neighbor site of Ti is much larger than at all other sites, even at the rather low concentration of 0.098%. The explanation of the influence of S and Y on the mobility of oxygen in terms of the residence time ratio is similar to the above discussion for Ti.

As already mentioned above, the case of the highest concentration (1.852%, one solute in a simulation cell consisting of $3 \times 3 \times 3$ bcc unit cells) does not correspond to a dilute alloy since there may be a kind of simultaneous interaction of the diffusing oxygen atom with the solute and its periodic image. This is illustrated in Fig. 7 by comparison with the situation in a AKMC cell containing $4 \times 4 \times 4$ bcc unit cells. Due to periodic boundary conditions the environment of the tenth-neighbor site in Fig. 7(a) differs from that in Fig. 7(b). In the $4 \times 4 \times 4$ cell as well as in larger cells this site has one neighbor with a fifth-neighbor distance to the solute, one neighbor with a ninth-neighbor distance (9b), and two neighbors with a distance to the foreign atom larger than the tenth-neighbor distance (denoted by 13 and 17b). In the smaller cell the considered site has only one neighbor with a distance to the solute larger than the tenth-neighbor distance (13) and one neighbor with a ninth-neighbor distance (9b), but two neighbors with a fifth-neighbor distance. This leads to a modification of the ratios between the jumps from and to the tenth-neighbor site while the ratios for the other sites within the tenth-neighbor shell remain unchanged. The ratio of the number of jumps between 10 and 5 to the number of jumps between 10 and 9b is depicted in Fig. 8, for the solutes of group 2 and 3 at a temperature of 600 and 800 K. For concentrations up to 0.781% this ratio has a constant

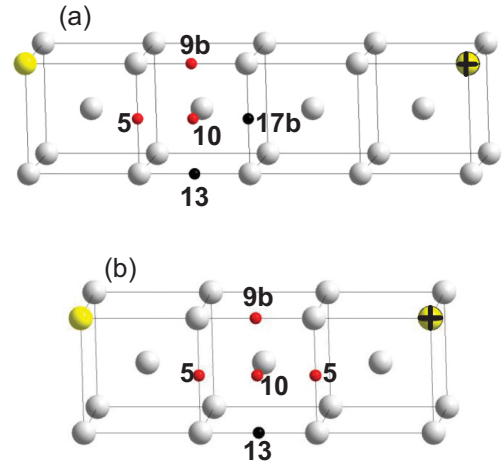

FIG. 7. Different environments of the tenth-neighbor octahedral site in a simulation cell consisting of $4 \times 4 \times 4$ (a) and $3 \times 3 \times 3$ (b) bcc unit cells. The figure illustrates the extensions of the simulation cell in one direction. In larger simulation cells the situation is similar to panel (a).

value which is determined by the given relation between the corresponding jump barriers. However, due to the situation discussed above, at the concentration of 1.852% the ratio becomes equal to two times the value obtained for the lower concentrations. At this concentration the highest ratio is found for Y and Ti. This leads to the intersection of the curves for the diffusion coefficient in Figs. 5(e) and 5(i). Such an intersection is not observed for the other solutes considered in Fig. 8. Obviously, the ratio of jump numbers at 1.852% is too low in these cases. Note that in Fig. 8 the data points are relevant whereas the lines are only shown to guide the eye. The above discussion illustrates a rather artificial example of a nondilute alloy and shows that in this case the diffusion coefficient may be higher than at lower concentrations. The

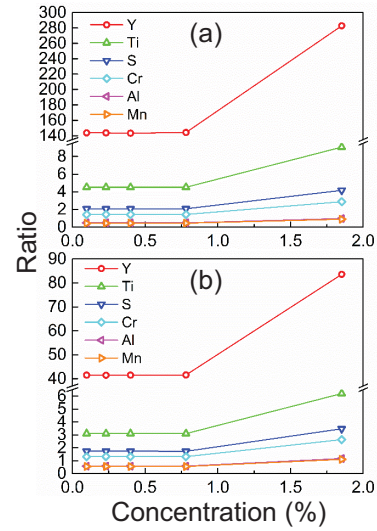

FIG. 8. Ratio of the number of oxygen jumps from 10 to 5 to the number of jumps between 10 and 9b as function of the solute concentration at 600 K (a) and 800 K (b).

general case of a nondilute alloy is not the subject of this paper. Here a huge number of additional barriers would have to be determined. These barriers concern all cases of possible simultaneous interactions of the oxygen atom with more than one substitutional solute.

Few experimental data on the diffusion of oxygen in iron are available, and they were already obtained many years ago. All of them were determined by internal oxidation measurements [42–45]. This method is based on the observation that solutes with a higher chemical affinity to oxygen than iron are preferentially oxidized. This leads to the formation of tiny precipitates or inclusions. In an oxygen-containing ambient, a layer with these precipitates is formed, starting from the sample surface. At a given temperature the square of the layer thickness increases linearly with time, and the rate depends on temperature according to an Arrhenius law. This suggests that the internal oxidation is mainly controlled by the diffusion of oxygen, and the diffusion coefficient can be determined by a theoretical analysis of the measured data. Al [42,44], Si [43], and Ti [45] solutes were considered, with concentrations between 0.1 and 1 wt. %. The experiments were performed mainly above the Curie temperature. In the temperature range between 1023 and 1173 K Takada *et al.* [43–45] obtained very similar data for the oxygen diffusion, independently of whether Al, Si, or Ti was used as the oxide forming solute. They described the oxygen diffusion coefficient by a simple Arrhenius formula with activation energy between 0.89 and 0.95 eV. In their investigations of the internal oxidation of Al solutes in bcc Fe Swisher and Turkdogan [42] used a different experimental procedure than Takada *et al.* and found an activation energy of about 1 eV. The experimental values of the diffusion coefficient of oxygen determined by internal oxidation are considerably lower than the theoretical results of the present paper. Also, the experimental activation energy is higher than the corresponding temperature-dependent values which can be obtained from Fig. 5. The fact that the measured data could be fitted to a simple Arrhenius relation might be due to the narrow temperature range which was investigated. The very weak dependence on the kind of solute is more surprising since a significant difference between Al, Si, and Ti is found by present theoretical investigations [see Figs. 5(a), 5(b), and 5(e)]. Therefore, one might conclude that the slow diffusion of oxygen observed in the internal oxidation experiments is dominated by the same type of strong traps which are not considered in the present paper. Such traps could be, e.g., dislocations. Assuming a dislocation density of 10^{12} m^{-2} the areal density per atom is about 0.000008%. This value is much lower than the concentration of solutes per atom considered in the cited experiments. However, the trapping efficiency of a dislocation is not yet known. Its calculation and the consideration of other traps should be the subject of future studies. On the other hand, in the polycrystalline samples used in experiments the grains were relatively large, and there was no evidence for an influence of grain boundaries on diffusion and internal oxidation [42]. Furthermore, in the analysis of the internal oxidation data it was assumed that all oxygen atoms from the ambient are consumed for oxidation of the solute. This is mainly because this part of the oxygen atoms can be detected by the analytical methods that were applied in the experiments. However, another part which does not contribute to oxidation but takes part in diffusion may also exist. In order to clarify the open questions mentioned above it is suggested to perform new experimental investigations using single-crystalline bcc Fe samples with high purity and a well-defined concentration of substitutional atoms, as well as low or varying dislocation density. In these measurements high-resolution analytical methods such as secondary ion mass spectrometry in combination with x-ray photoelectron spectroscopy [46] should be applied. In this manner the understanding of the complex processes involving diffusion of atoms and oxidation could be improved significantly.

IV. SUMMARY AND CONCLUSIONS

The effect of substitutional foreign atoms on oxygen diffusion in bcc Fe was investigated by a combination of DFT calculations and AKMC simulations. At first DFT was used to investigate three different migration paths of oxygen in pure bcc Fe, i.e., between first-neighbor, second-neighbor, and third-neighbor octahedral interstitial sites. Most relevant is the first-neighbor jump with a linear migration path and the tetrahedral interstitial site as the saddle point. The second-neighbor jump consists of two successive first-neighbor jumps. The third-neighbor jump has a nonlinear migration path and the saddle point corresponds to a rhombohedral interstitial site, but the barrier for such a direct jump is too high to be relevant for O diffusion. In the presence of a substitutional solute the migration path is rather similar to that in pure bcc Fe, i.e., from a modified octahedral site via a modified tetrahedral site to another modified octahedral site as the first-neighbor jump. The interaction of oxygen with Si, P, Ni, Mo, and W is primarily repulsive. The corresponding migration barriers are not very different from that in pure Fe, with the exception of a high barrier close to the substitutional atom. Al, S, Ti, Cr, Mn, and Y exhibit strong attractive interactions with oxygen, associated with large barriers for escape from neighbor shells close to the solute. The barriers for approaching the substitutional atom are frequently relatively low. In the vicinity of S and Ti the escape is impeded by the combined action of the barriers for $2 \rightarrow 5$ and for $5 \rightarrow 6$ or $5 \rightarrow 10$ jumps, while for Al, Mn, and Cr the combination of the barriers for the $1 \rightarrow 2$ and the $2 \rightarrow 5$ jump impedes the escape. Some peculiarities were found in the case of Y: A direct transition between neighbors 5 and 6 is not possible and a direct second-neighbor jump between 6 and 2 was considered. In the vicinity of Y the escape of the oxygen atom is strongly impeded by the combined action of the barriers for the $2 \rightarrow 5$ and $5 \rightarrow 10$ transitions.

AKMC simulations were applied to study O diffusion in dilute alloys with concentrations of foreign atoms up to 0.781 at. %. Si, P, Ni, Mo, and W have a very small effect on the oxygen diffusion coefficient. Al, Cr, and Mn cause a considerable reduction of oxygen mobility. The reason for this behavior is the so-called trapping mechanism due to the attractive interaction between the substitutional solute and O. Such a mechanism is also responsible for the huge decrease of the diffusion coefficient observed in the case of S, Ti, and Y. In all cases investigated the oxygen diffusion coefficient was still some orders of magnitude higher than that of the corresponding foreign atom. Therefore, the assumption that the substitutional solute can be considered to be immobile throughout the AKMC

simulations is justified. The influence of Al, Cr, Mn, S, Ti, and Y leads to strong deviations from the Arrhenius behavior of the oxygen diffusion coefficient. This is due to the significant temperature dependence of the ratio between residence times in the respective states. At the concentration of 1.852% a simultaneous interaction of the diffusing oxygen atom with the solute and its periodic image may occur. In this rather artificial example of a nondilute alloy a higher diffusion coefficient than at lower concentrations may be observed.

The results of the present investigations show a strong dependence of the oxygen diffusion coefficient on the kind of the substitutional atom. This changes the picture of oxygen diffusion in dilute ferritic iron alloys importantly. Future experimental work is required to study these dependencies in detail and to consider other trapping mechanisms which might compete with those considered in the present paper. In this context theoretical studies on the modification of oxygen diffusion by other traps than substitutional solutes may be useful.

ACKNOWLEDGMENTS

This work was financially supported by the Chinese Scholarship Council (File No. 201606240015). The authors thank very much Dr. Luca Messina (KTH Royal Institute of Technology and Universita Della Svizzera Italiana) for valuable comments. They are grateful to the Center for Information Services and High Performance Computing at Technische Universität Dresden and to the Department of Information Service and Computing at Helmholtz-Zentrum Dresden–Rossendorf for providing extensive computing time. The work also contributes to the Joint Programme on Nuclear Materials of the European Energy Research Alliance.

[1] C. S. Becquart and C. Domain, Phys. Status Solidi B **247**, 9 (2010).
[2] L. Messina, N. Castin, C. Domain, and P. Olsson, Phys. Rev. B **95**, 064112 (2017).
[3] D. Simonovic, C. K. Ande, A. I. Duff, F. Syahputra, and M. H. F. Sluiter, Phys. Rev. B **81**, 054116 (2010).
[4] P. Liu, W. Xing, X. Cheng, D. Li, Y. Li, and X.-Q. Chen, Phys. Rev. B **90**, 024103 (2014).
[5] C. Barouh, T. Schuler, C.-C. Fu, and T. Jourdan, Phys. Rev. B **92**, 104102 (2015).
[6] S. L. Shang, H. Z. Fang, J. Wang, C. P. Guo, Y. Wang, P. D. Jablonski, Y. Du, and Z. K. Liu, Corr. Sci. **83**, 94 (2014).
[7] C. J. Ortiz, M. J. Caturla, C. C. Fu, and F. Willaime, Phys. Rev. B **80**, 134109 (2009).
[8] P. Grigorev, D. Terentyev, G. Bonny, E. E. Zhurkin, G. van Oost, and J.-M. Noterdaeme, J. Nucl. Mater. **474**, 143 (2016).
[9] J. Svoboda, Y. V. Shan, E. Kozeschnik, and F. D. Fischer, Modell. Simul. Mater. Sci. Eng. **21**, 065012 (2013).
[10] G. R. Odette, JOM **66**, 2427 (2014).
[11] C. L. Fu, M. Krcmar, G. S. Painter, and X. Q. Chen, Phys. Rev. Lett. **99**, 225502 (2007).
[12] D. Murali, B. K. Panigrahi, M. C. Valsakumar, S. Chandra, C. S. Sundar, and B. Raj, J. Nucl. Mater. **403**, 113 (2010).
[13] A. Claisse and P. Olsson, Nucl. Instrum. Methods Phys. Res. B **303**, 18 (2013).
[14] G. Kresse and J. Hafner, Phys. Rev. B **47**, 558 (1993).
[15] G. Kresse and J. Furthmüller, Comput. Mater. Sci. **6**, 15 (1996).
[16] G. Kresse and J. Furthmüller, Phys. Rev. B **54**, 11169 (1996).
[17] P. E. Blöchl, Phys. Rev. B **50**, 17953 (1994).
[18] G. Kresse and D. Joubert, Phys. Rev. B **59**, 1758 (1999).
[19] J. P. Perdew, K. Burke, and M. Ernzerhof, Phys. Rev. Lett. **77**, 3865 (1996).
[20] H. J. Monkhorst and J. D. Pack, Phys. Rev. B **13**, 5188 (1976).
[21] M. Methfessel and A. T. Paxton, Phys. Rev. B **40**, 3616 (1989).
[22] H. Jonsson, G. Mills, and K. W. Jacobsen, *Classical and Quantum Dynamics In Condensed Phase Simulations* (World Scientific, Singapore, 1998), pp. 389–404.
[23] G. Henkelman, B. P. Uberuaga, and H. Jonsson, J. Chem. Phys. **113**, 9901 (2000).
[24] http://theory.cm.utexas.edu/vtsttools.
[25] P. Hänggi, P. Talkner, and M. Borkovec, Rev. Mod. Phys. **62**, 251 (1990).
[26] L. T. Kong and L. J. Lewis, Phys. Rev. B **74**, 073412 (2006).
[27] G. H. Vineyard, J. Phys. Chem. Solids **3**, 121 (1957).
[28] Y. Jiang, J. R. Smith, and G. R. Odette, Phys. Rev. B **79**, 064103 (2009).
[29] C. Barouh, T. Schuler, C.-C. Fu, and M. Nastar, Phys. Rev. B **90**, 054112 (2014).
[30] D. Murali, M. Posselt, and M. Schiwarth, Phys. Rev. B **92**, 064103 (2015).
[31] See Supplemental Material at http://link.aps.org/supplemental/10.1103/PhysRevB.98.064103 for data on volume changes and distortions, and on Bader analysis.
[32] http://theory.cm.utexas.edu/henkelman/code/bader/.
[33] L. Messina, M. Nastar, N. Sandberg, and P. Olsson, Phys. Rev. B **93**, 184302 (2016).
[34] M. Mock and K. Albe, J. Nucl. Mater. **494**, 157 (2017).
[35] L. Messina, M. Nastar, T. Garnier, C. Domain, and P. Olsson, Phys. Rev. B **90**, 104203 (2014).
[36] A. F. Voter, *Introduction to the Kinetic Monte Carlo Method* (Springer, New York, 2007), pp. 1–23.
[37] M. W. Guinan, R. N. Stuart, and R. J. Borg, Phys. Rev. B **15**, 699 (1977).
[38] M. Posselt, F. Gao, and D. Zwicker, Phys. Rev. B **71**, 245202 (2005).
[39] N. Anento, A. Serra, and Y. Osetsky, Acta Mater. **132**, 367 (2017).
[40] R. A. Oriani, Acta Metall. **18**, 147 (1970).
[41] H. Mehrer, N. Stolica, and N. A. Stolwijk, in *Diffusion in Solid Metals and Alloys*, edited by H. Mehrer (Springer-Verlag, Berlin, 1990).
[42] J. H. Swisher and E. T. Turkdogan, Trans. Met. Soc. AIME **239**, 426 (1967).
[43] J. Takada and M. Adachi, J. Mater. Sci. **21**, 2133 (1986).
[44] J. Takada, S. Yamamoto, S. Kikuchi, and M. Adachi, Oxid. Met. **25**, 93 (1986).
[45] J. Takada, S. Yamamoto, and M. Adachi, Z. Für Metallkde. **77**, 6 (1986).
[46] A. P. Grosvenor, B. A. Kobe, and N. S. McIntyre, Surf. Sci. **565**, 151 (2004).